

COMMUNICATION

[View Article Online](#)
[View Journal](#) | [View Issue](#)

Stability, surface features, and atom leaching of palladium nanoparticles: toward prediction of catalytic functionality[†]

Cite this: *Phys. Chem. Chem. Phys.*, 2013, **15**, 5488

Received 11th January 2013,
Accepted 4th March 2013

DOI: 10.1039/c3cp00135k

www.rsc.org/pccp

Hadi Ramezani-Dakhel,^a Peter A. Mirau,^b Rajesh R. Naik,^b Marc R. Knecht^c and Hendrik Heinz^{*a}

Surfactant-stabilized metal nanoparticles have shown promise as catalysts although specific surface features and their influence on catalytic performance have not been well understood. We quantify the thermodynamic stability, the facet composition of the surface, and distinct atom types that affect rates of atom leaching for a series of twenty near-spherical Pd nanoparticles of 1.8 to 3.1 nm size using computational models. Cohesive energies indicate higher stability of certain particles that feature an approximate 60/20/20 ratio of {111}, {100}, and {110} facets while less stable particles exhibit widely variable facet composition. Unique patterns of atom types on the surface cause apparent differences in binding energies and changes in reactivity. Estimates of the relative rate of atom leaching as a function of particle size were obtained by the summation of Boltzmann-weighted binding energies over all surface atoms. Computed leaching rates are in good qualitative correlation with the measured catalytic activity of peptide-stabilized Pd nanoparticles of the same shape and size in Stille coupling reactions. The agreement supports rate-controlling contributions by atom leaching in the presence of reactive substrates. The computational approach provides a pathway to estimate the catalytic activity of metal nanostructures of engineered shape and size, and possible further refinements are described.

The size and shape of colloidal metal nanostructures prepared by reductive synthesis from solution precursors can be customized

in the sub-5 nm range using biological, organic, and inorganic capping agents.^{1–4} The wide range of accessible metal nanostructures comprises, for example, near-spherical particles, rods, cubes, prisms, octahedra, tetrahedra, decahedra, and icosahedra. Applications in catalysts,^{5–11} sensors,^{12,13} and nanoelectronic devices¹⁴ have been explored, such as palladium (Pd) nanoparticles in carbon–carbon coupling reactions.^{5–11} In spite of many examples, details of the interfaces remain difficult to monitor in experiment. Thus, the influence of interfacial features on catalytic mechanisms and the efficiency of catalysts still remain unclear. There is consensus, however, that the nanoparticles provide surface atoms for the formation of organo-palladium compounds and perform catalytic functions.^{15–18} The aim of this work is a systematic analysis of the thermodynamic stability, surface structure, and rates of atom leaching for commonly observed, bare, near-spherical Pd nanoparticles as a function of size using computational models. We will also demonstrate for the example of Stille coupling reactions that such models and simple thermodynamic considerations of atom binding provide correlations with the observed catalytic efficiency for a series of known data and a pathway toward understanding the reactivity of other metal nanostructures.

Nascent atomic clusters of Pd and other noble metals remain amorphous up to a critical size of ~1.5 nm at room temperature upon reductive synthesis from soluble precursors and then crystallize into a fcc or similar crystalline structure.^{1,2,5,6} At the initial crystallization stages, usually cuboctahedra and truncated octahedra are formed.^{1,2,5,6} The emergent crystallites can also take the shape of Platonic solids, although only for a few “magic” numbers of atoms. The total energy of fcc metal particles larger than 200 atoms (>1.7 nm) is lowest for truncated octahedra and cuboctahedra due to a low ratio of surface area to volume and comparatively high coordination numbers of metal atoms on the surface.¹⁹ The production of near-spherical particles or cuboctahedra has also been demonstrated in the peptide-mediated synthesis of Pd nanoparticles.^{1,2,11} In these reactions, biotic–abiotic interactions control the size of the

^a Department of Polymer Engineering, University of Akron, Akron, Ohio, 44325, USA.
E-mail: hendrik.heinz@uakron.edu

^b Wright-Patterson Air Force Base, Nanostructured and Biological Materials Branch, Air Force Research Laboratory, Dayton, Ohio, 45433, USA

^c Department of Chemistry, University of Miami, Coral Gables, Florida, 33146, USA

[†] Electronic supplementary information (ESI) available: Details of particle shapes and atom types (Fig. S1), percentages of exposed atoms as a function of particle size (Fig. S2), computed leaching rate of palladium nanoparticles per surface area (Fig. S3), abstraction energies of all atoms for all nanoparticles (Table S1), details of computational and analysis procedures (Section S1), comparison of nanoparticle structure and cohesive energy to DFT calculations and experiment (Section S2), a discussion of mechanistic aspects and individual steps of Stille coupling reactions (Section S3), and supplementary references. See DOI: 10.1039/c3cp00135k

nanoparticles in a range from 1.8 to 3.1 nm by recognition of crystallographic features. While it may be difficult to obtain perfect particle geometries, the major products in aqueous solutions after nucleation and initial growth are pseudo-spherical particles composed of {111}, {100}, and {110} facets as well as cuboctahedra unless specific shape-directing agents are applied (Fig. 1).^{1,2,5,11,20}

For the analysis of surface and leaching properties, we employed computational models that reproduce bulk and surface properties, specific molecular recognition in solution, as well as nanoscale characteristics of alloys in accurate agreement with laboratory measurements (CHARMM-METAL).^{1,21–26} Atomistic models of the nanoparticles were constructed from an infinite fcc lattice by choice of a center atom and application of radial cutoffs from 9 Å to 15 Å in steps of 0.1 Å, followed by extensive molecular dynamics simulation to identify the structure of minimum energy for each particle at 298 K (Fig. 1a). We chose a lower size limit of 1.8 nm (225 atoms) and an upper size limit of 3.1 nm (1061 atoms) as in experiment for our analysis while the series may similarly continue for larger particles. Cohesive energies of the particles, normalized per atom, decrease toward larger negative values as the particle size increases (Fig. 1b). The decrease in cohesive energy with increasing radius r proceeds approximately as $1/r$ and reflects the diminishing ratio of surface atoms of higher energy ($\sim r^2$) to bulk atoms of lower energy ($\sim r^3$) for near-spherical particles. The trend agrees with DFT studies on smaller particles up to 309 atoms, although absolute values of cohesive energies are somewhat underestimated by the force field in comparison to experiment and DFT (see Section S2 in the ESI†).²⁷ Offsets from the master curve of cohesive energy *versus* size distinguish more stable particles from less stable particles. The origin of offsets are deviations from ideal spherical symmetry related to the discrete number of atoms per particle, including variations in the ratio of {111}, {100}, and {110} facets on the surface and the presence of adatoms in some cases. Seemingly small differences in cohesive energy from the master curve are significant; for example, an offset of 0.1 kcal per mol atoms (as in Fig. 1b) corresponds to a cumulative difference of 50 kcal mol⁻¹ for a particle containing 500 atoms.

The results show that only a fraction of particles below the master curve is thermodynamically stable (colored panels in Fig. 1a and colored data points in Fig. 1b). These particles exhibit mainly even facets, rarely show surface reconstruction in the simulation, and likely dominate the size distribution of synthesized particles. The other particles near or above the master curve are thermodynamically less stable (non-colored panels in Fig. 1a and black data points in Fig. 1b). These particles contain a higher number of under-coordinated surface atoms and adatoms with increased local mobility. The thermodynamically less stable particles are prone to surface reconstruction, reconstruction into different shapes, or disproportionation in size that lead to stabilization.^{1–3,11}

The analysis of surface structures shows that all near-spherical palladium nanoparticles are bounded by {111}, {100}, and {110} facets (Fig. 2). The majority of the surface is usually constituted

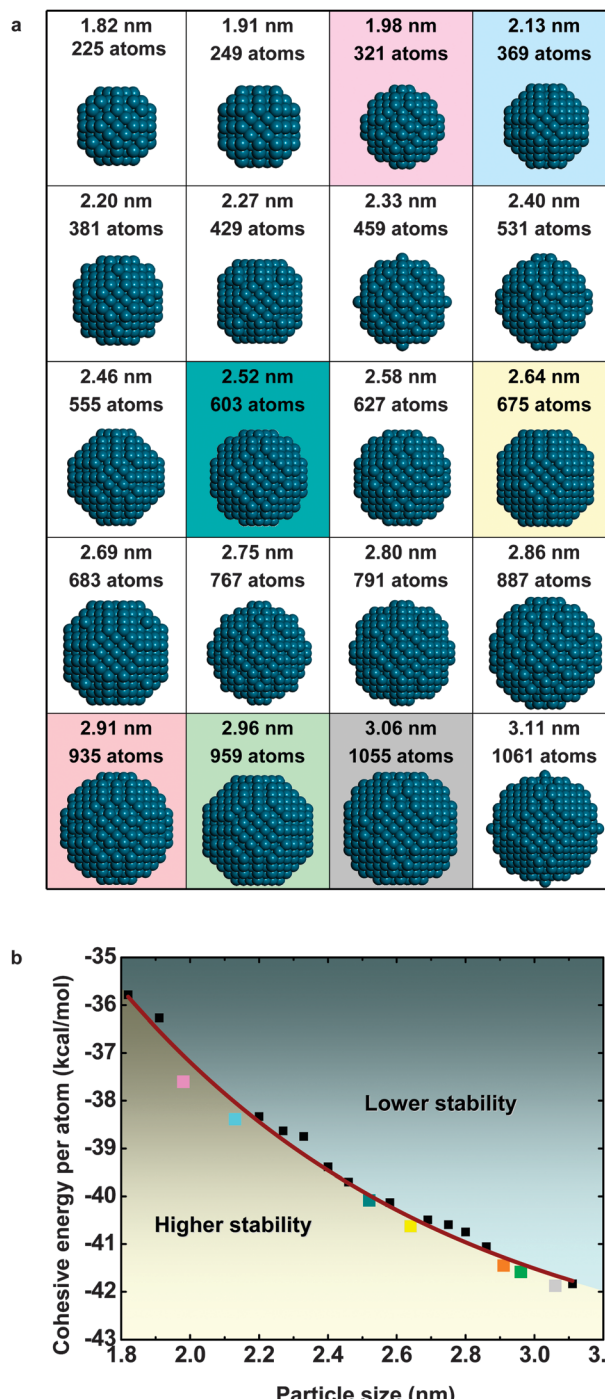


Fig. 1 (a) Surface features of near-spherical Pd nanoparticles of 1.8 nm to 3.1 nm size indicate variations in shape, facet composition, and in the occurrence of adatoms. Energetically more stable particles are highlighted on colored background. (b) The thermodynamic stability of near-spherical Pd nanoparticles can be assessed using the cohesive energy per atom computed by the CHARMM-METAL force field. The cohesive energy decreases as a function of particle size, whereby colored data points below the master curve identify particles of greater stability (highlighted in panel (a) on colored background), and data points above the master curve identify particles of lower stability.

by {111} facets of lowest surface energy, while facets of higher surface energy, *i.e.*, {100} and {110}, comprise a smaller fraction. Stable particles exhibit a similar percentage of {111} facets of ~60%,

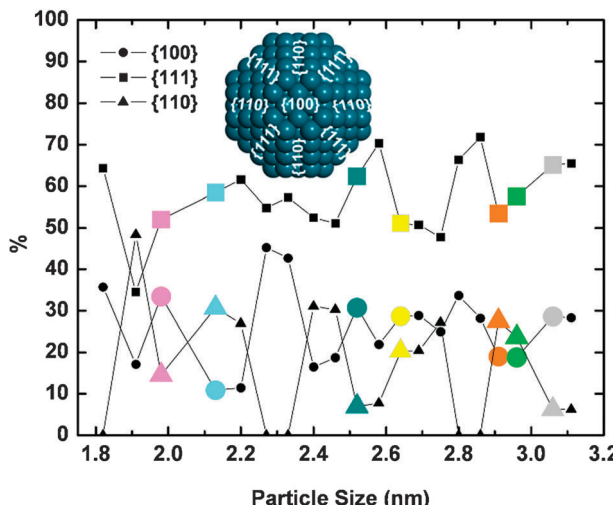


Fig. 2 The composition of the nanoparticle surface in percentages of {111}, {100}, and {110} facets for near-spherical particles of 1.8 nm to 3.1 nm size. The ratio of facets is similar for stable particles (larger colored symbols) and scatters over a wider range for less stable particles (smaller black symbols).

while the percentage of {100} and {110} facets varies, leading to compositions such as 60/10/30 (2.13 nm) to 65/30/5 (3.06 nm). Less stable particles display a wider range of variation such as 35/15/50 (1.91 nm) to 70/30/0 (2.86 nm) for the percentage of {111}, {100}, and {110} facets, respectively. Similarities in surface composition of stable particles are related to higher coordination numbers of Pd atoms and smaller surface area-to-volume ratio. The percentage of edge, vertex, and face atoms, in contrast, shows no uniform trend as a function of thermodynamic stability nor size of the particles (Fig. S2, ESI†).

At the level of individual atoms, the surface of each nanoparticle consists of subsets of chemically equivalent atoms that can be identified by symmetry (Fig. 3a and Fig. S1, ESI†). The resulting number of atom types (different color) increases for larger particles and ranges from 4 to 11 for the size range considered. The number of surface atoms of the same type (same color) per particle ranges from 6 to 48 depending on the facet composition and location of the atom within the host facet. The unique distribution of atom types for each nanoparticle captures differences in the surface structure that affect the reactivity and catalytic performance (Fig. 3a).

The atom type represents key characteristics such as the size and cohesive energy of the particle, the position of the atom on the surface, and its atomic coordination number. Not surprisingly, the atom type also uniquely determines the binding energy of an individual atom. We computed the abstraction energy of all atom types on the surface of each particle as the energy required to detach the atom from the surface by more than 1.2 nm (Fig. 3b and Section S1.6 in the ESI†). This energy can be compared to the free energy of atom leaching in C–C coupling reactions and varies from 30 to 69 kcal mol⁻¹ (Fig. 3c and Table S1, ESI†). The abstraction energy is lowest for adatoms, as found in unstable particles of 2.20, 2.33, 2.69, and 3.11 nm size (Fig. 1), that may disproportionate into more

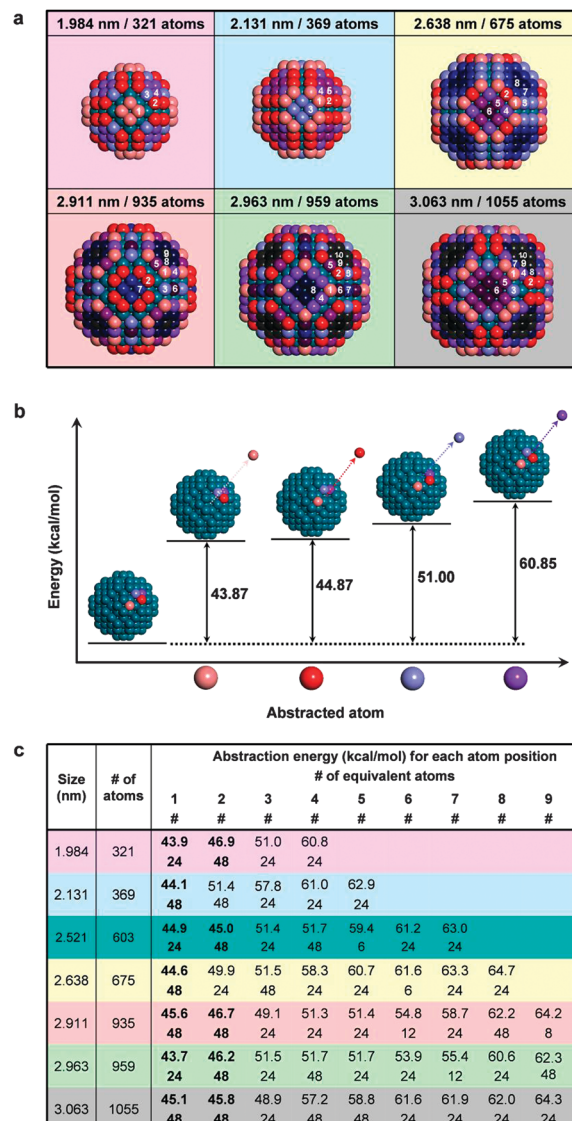


Fig. 3 (a) A highly specific pattern of chemically distinct atom types can be identified on the surface of each stable nanoparticle. The sequence of lighter to darker colors and increasing numbers correspond to increasing abstraction energies (see Fig. S1, ESI† for 2.52 nm particle). (b) Illustration of the abstraction energy as the difference between atoms bound and removed for a 1.9 nm particle. (c) Computed abstraction energies and number of equivalent atoms for each atom type j on the surface of stable nanoparticles. The designation of atom types ($j = 1, 2, \dots$) corresponds to the atom labels in panel (a). Only atoms of type 1 and 2 are removed from the surface with statistical significance and contribute to catalytic functionality (highlighted in bold).

stable particles by atom transfer mechanisms.²⁸ For stable particles, the abstraction energy of individual atoms ranges from 44 to 65 kcal mol⁻¹. Abstraction energies on stable particles are lowest for vertex atoms and edge atoms, and highest for face atoms. The abstraction energy for the most reactive atom types on stable particles still ranges over many multiples of RT ($1 RT = 0.6$ kcal mol⁻¹) and indicates that only atoms of lowest and second lowest abstraction energy may be leached at room temperature (Fig. 3c). The fingerprint of abstraction energies depends greatly on the nanoparticle symmetry and size,

even for atom types that appear similar at first sight. For example, abstraction energies of vertex atoms of stable particles vary up to 2 kcal mol⁻¹ and the binding energy of most accessible edge atoms is higher between 3 to 7 kcal mol⁻¹ (Fig. 3 and Table S1, ESI†). Besides, the percentages of vertex and edge atoms on the surface show no correlation with particle size (Fig. S2, ESI†).

Tests of the influence of water molecules on computed abstraction energies on selected systems showed no significant changes compared to vacuum. The strong cohesion of atoms to the metal surface is mainly related to the high surface tension of Pd in comparison to both water and vacuum (1980 mJ m⁻² versus 72 mJ m⁻² and 0 mJ m⁻²).²⁴ However, the solvent supports partial abstraction of individual atoms and accelerates atomic rearrangements on the surface following the abstraction, which will be explored in further work (see Section S1.6 in the ESI†).

The presence of surface atoms of different binding energy has important implications for the catalytic performance of Pd nanoparticles in Stille, Suzuki, and Heck coupling reactions (Fig. 4).^{15,16,29–32} To date, few details are known about individual reaction steps in the presence of nanoparticles, however, leaching of metal atoms has been suggested to be part of the reaction mechanism (see Section S3 in the ESI†).^{15–18} The models allow estimates of the relative rate of atom leaching R_N on bare metal nanoparticles using the abstraction energy and the number of least bound Pd atoms (Fig. 3c). The rates R_N for each nanoparticle were calculated assuming that (i) the activation free energy of abstraction of an individual atom equals the full abstraction energy, (ii) the total rate of abstraction R_N equals a summation of the Boltzmann-weighted abstraction energy E_i over all individual atoms $i = 1, 2, \dots, N_s$ on the nanoparticle surface, normalized by the total number of atoms N of each nanoparticle for comparison to rate measurements in experiment:³

$$R_N \sim \frac{1}{N} \sum_{i=1}^{N_s} e^{-\frac{E_i}{RT}} \quad (1)$$

(iii) a particular nanoparticle size reflects some effects of ligands and solvents in the synthesis which are otherwise neglected.

Details of the calculation can be found in Section S1.7 in the ESI†

The computed relative reaction rates of atom leaching for stable, bare nanoparticles correlate qualitatively well with measured catalytic turnover frequencies (TOFs) of peptide-covered nanoparticles in Stille coupling (Fig. 4a).³ The correspondence between simulation and measurements indicates that atom leaching could be the rate-determining step in the reaction mechanism (Fig. 4b) and also agrees with reported correlations between the number of leached atoms in solution and the reaction rate.³³ The highest computed rate estimate and measured TOF³ is found agreeably for nanoparticles of 2.13 nm size (Fig. 4a), which exhibit a high number of leachable atoms of low abstraction energy according to the model (Fig. 3c).

On the other hand, the amount of available reference data is sparse and several factors may contribute to the overall reaction rate. The size distribution of the particles is one such factor that we approximate in this initial study by the dominant particle size. The influence of a size distribution and a range of alternative particle shapes on leaching rates can be explored in further studies. Another important influence on the reaction rate is the activation barrier of individual reaction steps (Fig. 4b) that is affected by the coverage of the nanoparticle with ligands, choice of substrate, transmetalation agent, solvent, and reaction conditions. It is thus possible that diffusion of reagents to the particle surface,³ oxidative addition, transmetalation, and reductive elimination can affect the reaction rate (see Section S3 in the ESI†).^{15,16,18,34} Nevertheless, high barriers of 44 kcal mol⁻¹ for full atom detachment (1.2 nm) and still considerable barriers of 30 kcal mol⁻¹ for partial detachment (0.3 nm) support a rate-determining influence of atom leaching (see Section S1.7 in the ESI†). Activation energies for oxidative addition and transmetalation using ligand-based organo-Pd catalysts are only reported as 20–25 kcal mol⁻¹ by DFT calculations (unfortunately, no data are known for nanoparticle catalysts).^{35,36} When less reactive substrates were employed (Ar-Cl instead of Ar-I), the barriers were also shown to increase to 34 kcal mol⁻¹ and could then control the reaction rate.³⁶ It is thus

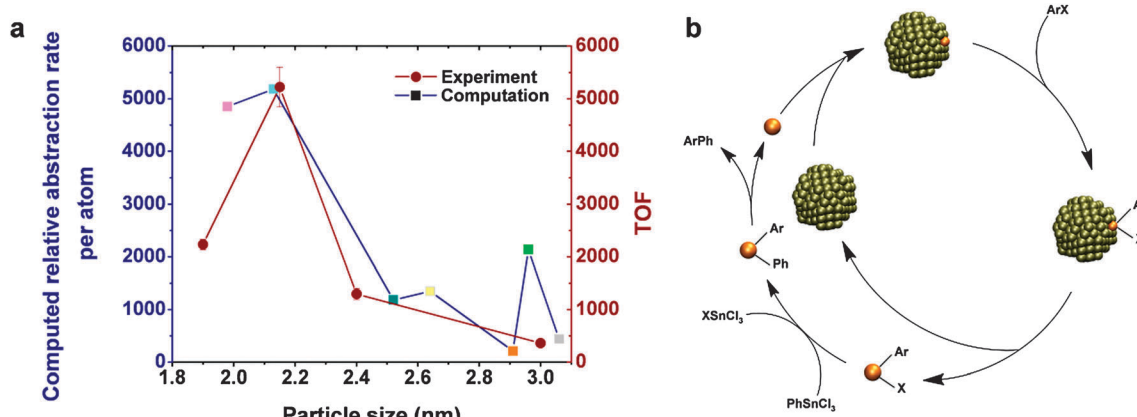


Fig. 4 (a) Correlation of the computed leaching rate of bare palladium nanoparticles with the measured catalytic turnover frequencies in Stille reactions as a function of nanoparticle size (TOF data from ref. 3). (b) Mechanism of the Stille reaction in the presence of palladium nanoparticle catalysts. Atom leaching following oxidative addition of the aryl halide Ar-X to the nanoparticle could be a rate-controlling step in the presence of reactive substrates.

conceivable that atom leaching can determine the reaction rate in the presence of reactive substrates and sufficient concentration of transmetalation agent (PhSnCl_3), though clearly further evidence will be needed. The reaction rate might also be affected by sequential leaching of multiple atoms from a nanoparticle once a defect has been created. Certainly, the computation of leaching rates using realistic particle models enables connections between surface features, particle size, and reactivity to examine the mechanism of coupling reactions and guide in the synthesis of nanometal catalysts with tailored reactivity.³

In summary, the analysis of surface features of palladium nanoparticles using atomistic models provides insight into specific atom types and enables estimates of leaching rates as a function of particle size that are difficult to obtain by laboratory measurements. It appears that atom abstraction could dominate the rate of nanoparticle-catalyzed carbon–carbon coupling reactions due to the high activation energy, although further rigorous evidence will be required. The computation of leaching rates can be applied to metal nanostructures of various sizes and shapes in future studies to develop and test hypotheses of reactivity in conjunction with laboratory data.

Acknowledgements

We are grateful for support by the Air Force Research Laboratory (FA8650-09-D-5037), UES, Inc. the National Science Foundation (HH: DMR-0955071, MK: CBET-1157431), the Ohio Supercomputing Center for provision of computational resources, and the University of Akron.

References

- 1 R. Coppage, J. M. Slocik, B. D. Briggs, A. I. Frenkel, H. Heinz, R. R. Naik and M. R. Knecht, *J. Am. Chem. Soc.*, 2011, **133**, 12346–12349.
- 2 C. Y. Chiu, Y. J. Li and Y. Huang, *Nanoscale*, 2010, **2**, 927–930.
- 3 R. Coppage, J. M. Slocik, M. Sethi, D. B. Pacardo, R. R. Naik and M. R. Knecht, *Angew. Chem., Int. Ed.*, 2010, **49**, 3767–3770.
- 4 C. Y. Chiu, Y. J. Li, L. Y. Ruan, X. C. Ye, C. B. Murray and Y. Huang, *Nat. Chem.*, 2011, **3**, 393–399.
- 5 B. Lim, M. J. Jiang, J. Tao, P. H. C. Camargo, Y. M. Zhu and Y. N. Xia, *Adv. Funct. Mater.*, 2009, **19**, 189–200.
- 6 Y. J. Xiong, H. G. Cai, B. J. Wiley, J. G. Wang, M. J. Kim and Y. N. Xia, *J. Am. Chem. Soc.*, 2007, **129**, 3665–3675.
- 7 N. T. S. Phan, M. Van Der Sluys and C. W. Jones, *Adv. Synth. Catal.*, 2006, **348**, 609–679.
- 8 J. K. Stille, *Angew. Chem., Int. Ed. Engl.*, 1986, **25**, 508–523.
- 9 C. Ornelas, J. Ruiz, L. Salmon and D. Astruc, *Adv. Synth. Catal.*, 2008, **350**, 837–845.
- 10 B. Lim, Y. J. Xiong and Y. N. Xia, *Angew. Chem., Int. Ed.*, 2007, **46**, 9279–9282.
- 11 R. Coppage, J. M. Slocik, B. D. Briggs, A. I. Frenkel, R. R. Naik and M. R. Knecht, *ACS Nano*, 2012, **6**, 1625–1636.
- 12 Z. F. Kuang, S. N. Kim, W. J. Crookes-Goodson, B. L. Farmer and R. R. Naik, *ACS Nano*, 2010, **4**, 452–458.
- 13 J. M. Slocik, J. S. Zabinski, D. M. Phillips and R. R. Naik, *Small*, 2008, **4**, 548–551.
- 14 D. Vanmaekelbergh, *Nat. Nanotechnol.*, 2009, **4**, 475–476.
- 15 A. K. Diallo, C. Ornelas, L. Salmon, J. R. Aranzaes and D. Astruc, *Angew. Chem., Int. Ed.*, 2007, **46**, 8644–8648.
- 16 D. B. Pacardo, J. M. Slocik, K. C. Kirk, R. R. Naik and M. R. Knecht, *Nanoscale*, 2011, **3**, 2194–2201.
- 17 A. d. Meijere and F. o. Diederich, *Metal-catalyzed cross-coupling reactions*, Wiley-VCH, Weinheim, 2004.
- 18 A. Biffis, M. Zecca and M. Basato, *J. Mol. Catal. A: Chem.*, 2001, **173**, 249–274.
- 19 D. J. Wales, *Energy landscapes*, Cambridge University Press, Cambridge, UK, New York, 2003.
- 20 F. Baletto, R. Ferrando, A. Fortunelli, F. Montalenti and C. Mottet, *J. Chem. Phys.*, 2002, **116**, 3856–3863.
- 21 J. Feng, J. M. Slocik, M. Sarikaya, R. R. Naik, B. L. Farmer and H. Heinz, *Small*, 2012, **8**, 1049–1059.
- 22 J. Feng, R. B. Pandey, R. J. Berry, B. L. Farmer, R. R. Naik and H. Heinz, *Soft Matter*, 2011, **7**, 2113–2120.
- 23 V. Petkov, B. N. Wanjala, R. Loukrakpam, J. Luo, L. F. Yang, C. J. Zhong and S. Shastri, *Nano Lett.*, 2012, **12**, 4289–4299.
- 24 H. Heinz, R. A. Vaia, B. L. Farmer and R. R. Naik, *J. Phys. Chem. C*, 2008, **112**, 17281–17290.
- 25 H. Heinz, T.-J. Lin, R. K. Mishra and F. S. Emami, *Langmuir*, 2013, **29**, 1754–1765.
- 26 L. Ruan, H. Ramezani-Dakhel, C.-Y. Chiu, E. Zhu, Y. Li, H. Heinz and Y. Huang, *Nano Lett.*, 2013, **13**, 840–846.
- 27 P. Nava, M. Sierka and R. Ahlrichs, *Phys. Chem. Chem. Phys.*, 2003, **5**, 3372–3381.
- 28 C. C. Cassol, A. P. Umpierre, G. Machado, S. I. Wolke and J. Dupont, *J. Am. Chem. Soc.*, 2005, **127**, 3298–3299.
- 29 D. L. Feldheim and C. A. Foss, *Metal nanoparticles: synthesis, characterization, and applications*, Marcel Dekker, New York, 2002.
- 30 A. H. M. de Vries, F. J. Parlevliet, L. Schmieder-van de Vondervoort, J. H. M. Mommers, H. J. W. Henderickx, M. A. M. Walet and J. G. de Vries, *Adv. Synth. Catal.*, 2002, **344**, 996–1002.
- 31 A. H. M. de Vries, J. M. C. A. Mulders, J. H. M. Mommers, H. J. W. Henderickx and J. G. de Vries, *Org. Lett.*, 2003, **5**, 3285–3288.
- 32 R. Narayanan, C. Tabor and M. A. El-Sayed, *Top. Catal.*, 2008, **48**, 60–74.
- 33 S. S. Prockl, W. Kleist, M. A. Gruber and K. Kohler, *Angew. Chem., Int. Ed.*, 2004, **43**, 1881–1882.
- 34 A. d. Meijere and F. Diederich, *Metal-catalyzed cross-coupling reactions*, Wiley-VCH, Weinheim, 2004.
- 35 R. Alvarez, O. N. Faza, A. R. de Lera and D. J. Cardenas, *Adv. Synth. Catal.*, 2007, **349**, 887–906.
- 36 L. Q. Xue and Z. Y. Lin, *Chem. Soc. Rev.*, 2010, **39**, 1692–1705.